CH-09-018

Determining Off-Normal Solar Optical Properties of Insect Screens

Nathan A. Kotey
Student Member ASHRAE

John L. Wright, PhD, PEng
Member ASHRAE

Michael R. Collins, PhD
Associate Member ASHRAE

ABSTRACT

Shading attachments may have a strong influence on solar gain. The determination of off-normal solar optical properties of individual layers of glazing/shading systems is required in order to estimate this solar gain, which influences building peak load and annual energy consumption. Recently, a unique test method was developed for the experimental determination of off-normal solar optical properties of flat shading devices (e.g., drapery fabrics and roller blinds). The study described in this research applies the same method to insect screens. More specifically, semi-empirical models were developed from measured data, obtained at varying angles of incidence using an integrating sphere installed in a spectrophotometer. The measurements were taken on six samples of screen material with various mesh sizes and wire reflectances. The measured data were compared with analytical models recently developed from geometry and ray tracing techniques. The results of this study demonstrate the reliability of using special sample holders attached to an integrating sphere to obtain off-normal solar optical properties of flat shading materials.

INTRODUCTION

Building energy consumption constitutes approximately 40% of the total energy used in the US (DOE 2004). It has also been estimated that about 25 billion dollars per year is tied to the thermal performance of windows (DOE 2004). Due to rising costs of conventional hydrocarbon fuels, there is an increased interest in conversion from conventional to clean and environmentally friendly sources of energy. The first step in this conversion is conservation. Improved thermal performance of windows, therefore, offers great potential.

In pursuit of energy conservation, shading devices such as venetian blinds, roller blinds, and draperies can be used to control solar gain. Their potential for reduction of cooling load and annual energy consumption is recognised to be large (e.g., Grasso and Buchanan [1982] and Harrison and van Wonderen [1998]). In addition, insect screens are frequently attached to windows, particularly in residential buildings, and recent studies have revealed that insect screens have a significant influence on solar gain (e.g., Brunger et al. [1999]). By using a solar simulator-based test method, Brunger et al. (1999) noted that a typical insect screen attached to a window reduced its solar heat gain coefficient (SHGC) significantly. Their test results showed that when the insect screen was placed on the outdoor side of a double-glazed window, SHGC was reduced by 46%. On the other hand, SHGC was reduced by 15% when the insect screen was placed on the indoor side of the window. In light of the aforementioned observations, an insect screen can be classified as a shading device and could be used to control solar gain.

Shading layers are often characterised by the assumption that each layer, whether homogeneous or not, can be represented by an equivalent homogenous layer that is assigned spatially averaged "effective" optical properties. This characterization of shading layers was used in a number of studies (e.g., Parmelee and Aubele [1952], Farber et al. [1963], Pfrommer et al. [1996], and Yahoda and Wright [2005]) and was shown to provide accurate optical properties of venetian blinds (Kotey et al. 2008).

The use of effective optical properties and a beam/diffuse split of solar radiation in multilayer systems provide virtually unlimited freedom to consider different types of shading

Nathan A. Kotey is a graduate student, **John L. Wright** is a professor, and **Michael R. Collins** is an associate professor in the Department of Mechanical and Mechatronics Engineering, University of Waterloo, Waterloo, Ontario, Canada.

layers. This approach also delivers the computational speed needed in the context of building energy simulation.

The most recent characterisation of screens is reported in the EnergyPlus reference manual (DOE 2007). Off-normal solar property models were developed for building energy simulation using analytical and ray tracing techniques. The models are based on the orthogonal crossed cylinder geometry with known wire diameter, wire centre-to-centre spacing, and wire reflectance. The models assume that the wire diameter and wire spacing are the same in both directions. For a unit of incoming beam radiation with known direction, the models account for both undisturbed flux going through the openings of the screen and intercepted flux. More specifically, the undisturbed flux constitutes the beam-beam transmittance. The portion of the intercepted flux that is not absorbed is scattered and leaves the layer as an apparent reflection or transmission. The portion of the intercepted flux not absorbed and emerging in the forward direction gives rise to beam-diffuse transmittance, and the flux emerging in the reverse direction is the beam-diffuse reflectance. The beam-diffuse transmittance model was "empirically" formulated by curve-fitting results from an optical ray tracing algorithm. The ray tracing algorithm is based on the assumption that the wire reflectance is diffuse. The beam-diffuse reflectance is a function of the beam-beam transmittance, the wire reflectance, and the beam-diffuse transmittance. The diffuse-diffuse transmittance and reflectance models are simply hemispherical integrations of the beam-total (beam-beam plus beam-diffuse) transmittance and beam-diffuse reflectance, respectively.

A measurement technique was devised to obtain the off-normal solar optical properties of flat shading devices (Kotey et al. 2009a, 2009b). It involves the use of special sample holders attached to an integrating sphere installed in a commercially available spectrophotometer. The integrating sphere is particularly useful since it can separate the undisturbed and scattered components of incident beam radiation. Cosine power functions were used to approximate the measured solar properties. The cosine power function was chosen for several reasons, including simplicity. The cosine function is also symmetrical, having zero gradient at $\theta = 0$ (normal incidence). It has maximum and minimum values at $\theta = 0$ and at $\theta = 90°$, respectively. Also, the shape of the curve can be modified by changing the value of the exponent. Given the solar optical properties at normal incidence, the semi-empirical models were developed to characterise the off-normal properties of drapery fabrics and roller blind materials (Kotey et al, 2009a, 2009b).

This paper summarises the results of research that used the same measurement technique to determine the off-normal solar optical properties of insect screens. The solar optical properties models obtained in this study can be used in multi-layer glazing/shading layer calculation modules of building energy simulation tools. To further demonstrate the reliability of the measurement technique, measured data were compared with analytical models, showing good agreement.

Table 1. Description of Insect Screen Samples

Item	Mesh Size, per in.^{2} (cm^2)	Wire Diameter, in. (cm)	Wire Spacing, in. (cm)	Colour
a	150 (23)	0.0026 (0.0066)	0.0067 (0.0170)	gray
b	120 (19)	0.0026 (0.0066)	0.0084 (0.0213)	gray
c	20 (3)	0.0160 (0.0406)	0.0518 (0.1315)	gray
d	60 (9)	0.0045 (0.0114)	0.0169 (0.0429)	gray
e	20 (3)	0.0100 (0.0254)	0.0521 (0.1323)	blue-gray
f	26 (4)	0.0060 (0.0152)	0.0414 (0.1052)	charcoal-black

TEST SAMPLES

Measurements were taken using six different samples of screens, as summarised in Table 1. Each screen is made of stainless steel wires that are woven to form an orthogonal mesh. The wires can be woven loosely, leaving significant open areas, or woven tightly with small openings. The screen samples considered represent a wide range of geometry and wire reflectances. Samples a through d are made of unpainted stainless steel wire with a metallic gray surface. Samples e and f are commercially produced insect screens with colored surfaces. The samples are shown in Figure 1.

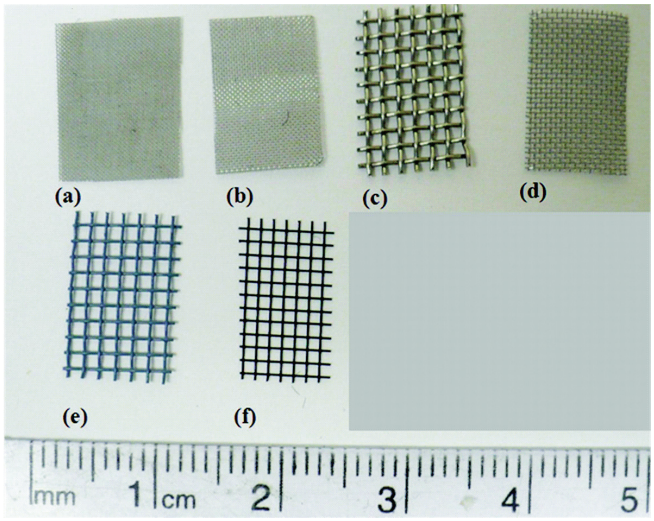

Figure 1 *Insect screen samples: a)150 mesh, gray; b) 120 mesh, gray; c) 20 mesh, gray; d) 60 mesh, gray; e) 20 mesh, blue-gray; f) 26 mesh, charcoal-black.*

When beam radiation is incident on the surface of an insect screen, it is split into two portions: the undisturbed portion transmitted through the openings and the intercepted portion—some of which will be scattered in the forward direction (i.e., transmitted) or scattered in the reverse direction (i.e., reflected). The scattered components, regardless of their true directional nature, are categorised as purely diffuse. This is done because the models presented here will be used within a multilayer glazing/shading model where beam and diffuse components of solar radiation are tracked (Wright and Kotey 2006). The undisturbed portion constitutes the beam-beam (specular) transmittance, τ_{bb}. At normal incidence, τ_{bb} is equivalent to the openness factor, $A_o = \tau_{bb}(\theta = 0)$, defined as the ratio of the open area to the total area of the material. The intercepted radiation is scattered by multiple reflections between the wires. The portion of the intercepted radiation that is not absorbed by the wires subsequently emerges in the forward direction as beam-diffuse transmittance, τ_{bd}, or in the backward direction as beam-diffuse reflectance, ρ_{bd}. The beam-total transmittance, τ_{bt}, is the sum of τ_{bb} and τ_{bd}. Reflectance measurements show that insect screens generally have a negligible specular component; hence, the beam-beam (specular) reflectance, ρ_{bb}, is zero. The beam-total reflectance is therefore equal to the beam-diffuse reflectance, $\rho_{bt} = \rho_{bd}$. Incident diffuse radiation is presumed to remain diffuse in transmission or reflection and the corresponding diffuse-diffuse properties are ρ_{dd} and τ_{dd}.

EXPERIMENTAL PROCEDURE

The experiments were performed with an integrating sphere (IS) attached to a double beam, direct ratio recording, rapid scanning spectrophotometer. The IS is a hollow, 110 mm (4.33 in.) diameter sphere with a highly reflective inner surface. This surface is designed to give uniformly diffuse reflection so that any light entering the sphere is uniformly distributed over the entire inner surface, eliminating any directional effects. Radiation detectors attached to a small opening on the sphere wall receive an integrated signal proportional to the rate at which radiant energy enters the sphere. The operational wavelength range of the IS is 0.25–2.5 μm, which covers almost 98% of the total solar spectrum.

Special sample holders that enable transmittance and reflectance measurements at off-normal incidence were fabricated from aluminium tubes with one end machined at a known angle, θ. They were installed in either the transmission or the reflection port, and they projected into the sphere. The length of each sample holder was such as to allow only the angled portion to project into the sphere. With a highly polished exterior surface, signal losses due to absorption on the exterior surfaces of the sample holders were minimised. Moreover, the interior surfaces of the sample holders were painted black in order to absorb radiation scattered in reflection during a transmittance measurement or scattered in transmission during a reflectance measurement. For each screen sample considered, spectral beam-beam transmittance τ_{bb}, beam-diffuse transmittance τ_{bd}, and beam-diffuse reflectance ρ_{bd} measurements were obtained at θ ranging from 0° to 60° in 15° steps.

Typical arrangements for transmittance and reflectance measurements are shown in Figure 2. To augment the IS measurements, a transmittance tray with a specially designed rotatable sample holder was used. With this arrangement, spectral beam-beam transmittance measurements were obtained at incidence angles ranging from 0° to 80°. In addition to validat-

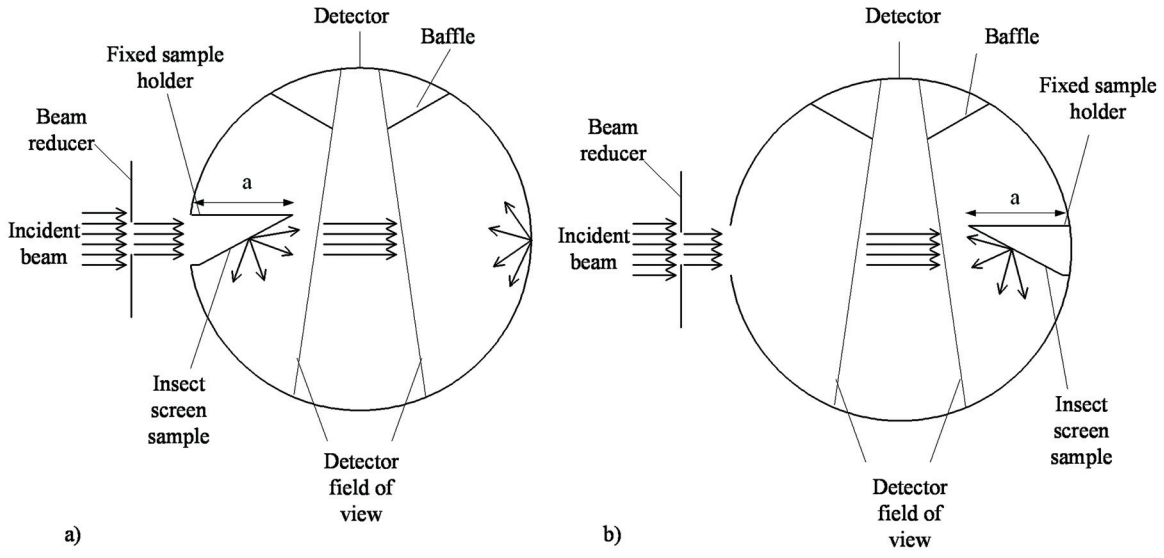

Figure 2 *Measurements with integrating sphere: a) off-normal transmittance measurements, b) off-normal reflectance measurements.*

ing IS measurements, the rotatable sample holder gave much needed information on the transmittance at grazing angles of incidence. The uncertainty in the measurements with the IS was estimated to be ±0.03 at a 95% confidence level. Error bars representing the level of measurement uncertainty are shown on the beam-total transmittance data of 60 mesh, 0.0045 in. (0.1143 mm) diameter, stainless steel in Figure 6. Details of the calibration, measurement procedure, and uncertainty estimates can be found in Kotey et al. (2009a, 2009b).

After the spectral measurements were obtained, solar optical properties were calculated using the 50-point selected ordinate method as described in ASTM E903-96 (ASTM 1996). The solar irradiance distribution (ASTM 1987) was divided into 50 equal-energy wavelength intervals. The spectral optical property was then evaluated at the centroidal wavelength of each interval.

SEMI-EMPIRICAL MODELS

Beam-Beam Transmittance Model

The geometric configuration of a screen is relatively simple and can be represented by orthogonal crossed wires with known wire diameter, *D*, and centre-to-centre spacing, *S* (see Figure 3). Assuming *D* and *S* are the same in both directions, then the openness A_o, defined as the portion of the screen area open to radiation at normal incidence, is

$$A_o = \frac{(S-D)^2}{S^2} \quad . \tag{1}$$

As stated previously, A_o is equivalent to beam-beam transmittance at normal incidence, $A_o = \tau_{bb}(\theta = 0)$. Thus, A_o can either be determined from geometry or by simply measuring $\tau_{bb}(\theta = 0)$. Another parameter of practical importance is the incidence angle beyond which direct beam transmission is cut off, θ_{cutoff}. From geometry, θ_{cutoff} can be estimated as:

$$\cos(\theta_{cutoff}) = \frac{D}{S} \tag{2}$$

This analysis establishes the endpoints of a curve that represents the beam-beam transmittance model. To obtain the shape of the curve, we use the cosine power function with an exponent selected to match the experimental data (e.g., Kotey et al. [2009a, 2009b]).

A convenient way to normalise τ_{bb} in order to represent a cosine power function with an exponent, *b*, is given by Equation 3:

$$^{\text{norm}}\tau_{bb} = \frac{\tau_{bb}(\theta)}{\tau_{bb}(\theta = 0)} = \cos^b\left(\frac{\theta}{\theta_{cutoff}} \cdot 90°\right) \tag{3}$$

For a given sample, a unique value of *b* allows the empirical function to match the experimental data, as shown in Figure 4. Assuming that *b* is a function of $\tau_{bb}(\theta = 0)$, a scatter graph of *b* versus $\tau_{bb}(\theta = 0)$ can be represented by a line, as shown in Figure 5. This line is given by

$$b = -0.45\ln(\text{MAX}(\tau_{bb}(\theta = 0), 0.01)) + 0.1 \quad . \tag{4}$$

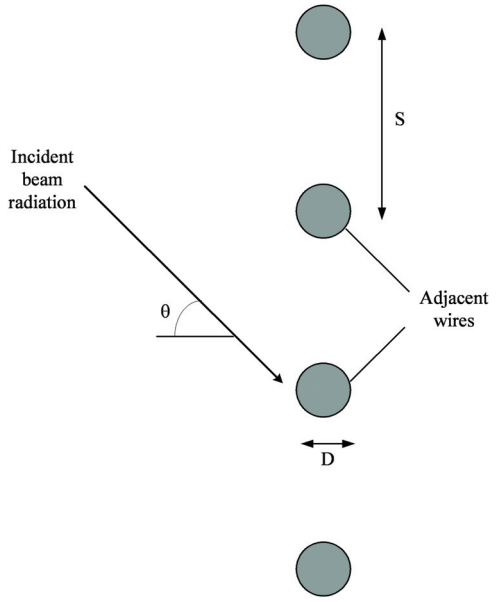

Figure 3 *Geometry used for insect screens.*

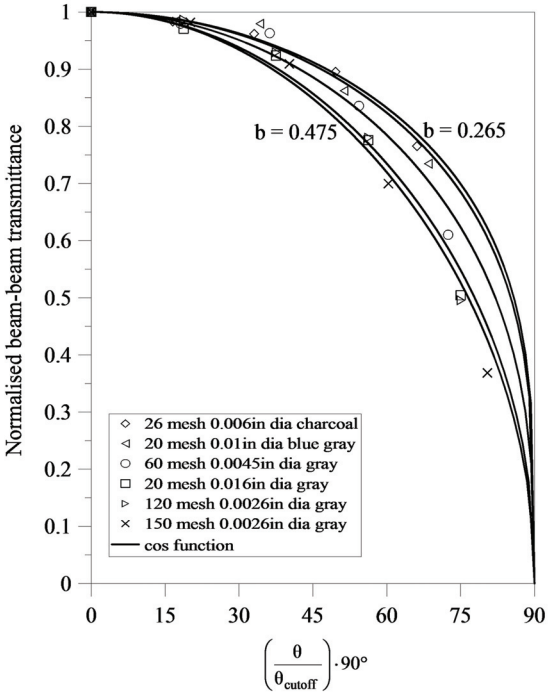

Figure 4 *Normalised beam-beam transmittance versus incidence angle (from measurements with the integrating sphere).*

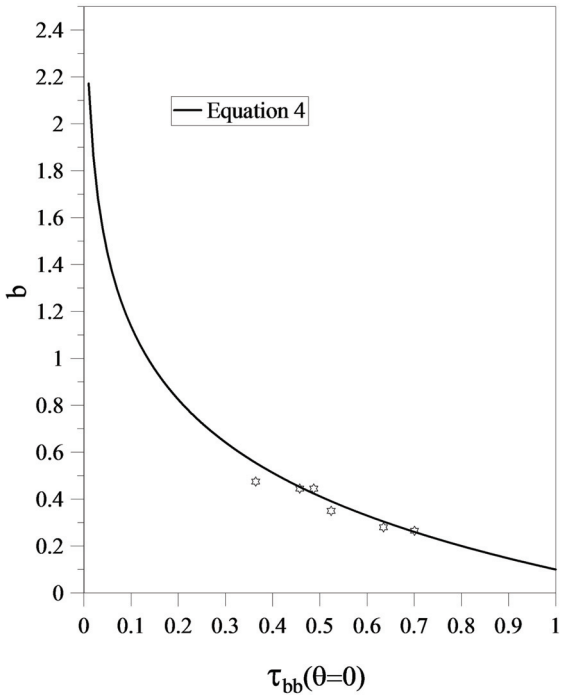

Figure 5 *Graph of b versus* $\tau_{bb}(\theta = 0)$.

Ideally, Equation 4 would be formulated such that b approaches zero as openness approaches 100%. In this limit, the insect screen disappears and Equation 3 applies no off-normal adjustment. However, some compromise was needed in order to retain the simplicity of the model and to retain the realism that the absorptivity of the screen remains between zero and unity for all possible input values.

More formally, Equations 1 through 4 can be used to calculate $\tau_{bb}(\theta)$ as function of $\tau_{bb}(\theta = 0)$ using:

$$\begin{aligned} \tau_{bb}(\theta) &= \tau_{bb}(\theta = 0)\cos^{b}\left(\frac{\theta}{\theta_{cutoff}} \cdot 90°\right) && \theta < \theta_{cutoff} \\ \tau_{bb}(\theta) &= 0 && \theta \geq \theta_{cutoff} \end{aligned} \quad (5)$$

Beam-Total Transmittance Model

The beam-total transmittance, τ_{bt} is the sum of τ_{bd} and τ_{bb}. A recent analytical model of screens (DOE 2007) reveals that τ_{bd} increases monotonically to a maximum value at θ_{cutoff} and then decreases sharply to zero at $\theta = 90°$. Since $\tau_{bb} = 0$ at $\theta_{cutoff} < 90°$ and $\tau_{bd} = 0$ at $\theta = 90°$, it implies that $\tau_{bt} = 0$ at $\theta = 90°$. We can represent the normalised form of τ_{bt} with a function given by Equation 6:

$$^{\text{norm}}\tau_{bt} = \frac{\tau_{bt}(\theta)}{\tau_{bt}(\theta = 0)} = \cos^{b}(\theta) \quad (6)$$

By inspection, the desired values of b can be obtained by working with Equation 6. Assuming b is a function of $\tau_{bt}(\theta = 0)$, a relation between b and $\tau_{bt}(\theta = 0)$ can be represented by

$$b = -0.65\ln(\text{MAX}(\tau_{bt}(\theta = 0), 0.01)) + 0.1 \; . \quad (7)$$

Similar to the way in which Equation 4 was formulated, some compromise was accepted in order that the model would provide realistic results in the extreme cases of insect screens with very high openness and very low reflectance.

Rearranging Equation 6,

$$\tau_{bt}(\theta) = \tau_{bt}(\theta = 0)\cos^{b}(\theta) \; . \quad (8)$$

Beam-Diffuse Transmittance Model

At any given θ, τ_{bd} is the difference between τ_{bt} and τ_{bb}. Thus,

$$\tau_{bd}(\theta) = \tau_{bt}(\theta) - \tau_{bb}(\theta) \, . \quad (9)$$

Beam-Total Reflectance Model

Measurements showed that the beam-total reflectance of the screen, ρ_{bt}, includes no appreciable specular component; thus, $\rho_{bt} = \rho_{bd}$.

In order to make an approximate distinction between wires of different reflectivity, an apparent wire reflectance, ρ^{w}, was defined such that

$$\rho_{bt}(\theta = 0) = \rho^{w}(1 - A_o) \, . \quad (10)$$

The reflectance model described by Equation 10 considers reflection at the surface of the wire as well as multiple reflections between the wires. Rearranging Equation 10,

$$\rho^{w} = \frac{\rho_{bt}(\theta = 0)}{1 - A_o} \; . \quad (11)$$

Equation 12 was used to define normalised beam-total reflectance:

$$^{\text{norm}}\rho_{bt}(\theta) = \frac{\rho_{bt}(\theta) - \rho_{bt}(\theta = 0)}{\rho_{bt}(\theta = 90°) - \rho_{bt}(\theta = 0)} \quad (12)$$

A model was then developed by comparing measurements with the function shown in Equation 13. Knowing only the openness of the screen and $\rho_{bt}(\theta = 0)$, the off-normal reflectance of the screen can be calculated as follows:

$$^{\text{norm}}\rho_{bt}(\theta) = 1 - \cos^{b}(\theta) \quad (13)$$

where

$$\rho_{bt}(\theta = 90°) = \rho_{bt}(\theta = 0) + (1 - \rho_{bt}(\theta = 0)) \cdot (0.35\rho^{w}) \; . \quad (14)$$

The exponent b was estimated for each set of experimental data by inspection, similar to the way in which values of b were found for the τ_{bb} model, and was found to correlate well with respect to ρ^{w}:

$$b = -0.45\ln(\rho^{w}) \; . \quad (15)$$

Finally, $\rho_{bt}(\theta)$ is obtained by combining Equations 12 and 13:

$$\rho_{bt}(\theta) = \rho_{bt}(\theta = 0) + (\rho_{bt}(\theta = 90°) - \rho_{bt}(\theta = 0))\ (1 - \cos^{b}(\theta)) \quad (16)$$

Diffuse-Diffuse Transmittance and Reflectance Models

The solar optical properties for incident diffuse radiation can be obtained by integrating the beam-total properties over the hemisphere. The diffuse-diffuse transmittance is

$$\tau_{dd} = 2\int_{0}^{\frac{\pi}{2}} \tau_{bt}(\theta)\sin(\theta)\cos(\theta)d\theta \ . \quad (17)$$

Similarly, the diffuse-diffuse reflectance is

$$\rho_{dd} = 2\int_{0}^{\frac{\pi}{2}} \rho_{bt}(\theta)\sin(\theta)\cos(\theta)d\theta \ . \quad (18)$$

Numerical integration can be used to evaluate the integrals in Equations 17 and 18.

DISCUSSION

Table 2 gives a summary of the measured normal incidence solar optical properties of screens considered in this study. Items a through f are the different screens as specified in Table 1. The results in Table 2 include measurements with and without the IS as well as A_o calculated from geometry. As expected, $\tau_{bb}(\theta = 0)$ obtained from measurements compared favourably with A_o. This observation clearly demonstrates the reliability of measuring A_o using a spectrophotometer.

Figures 6 through 9 show the variation of the solar optical properties with θ. The symbols represent measurements while the solid lines represent the semi-empirical models. Tables of measurement results are included in the Appendix. Clearly, there is a good agreement between measured and calculated results. As seen in Figure 6, τ_{bb} decreases as θ increases and falls to zero at θ_{cutoff}, which is directly dependent on D and S as given by Equation 2. Figure 7 also shows a decrease in τ_{bt} as θ increases, and in this case the semi-empirical model predicts a complete attenuation of τ_{bt} at $\theta = 90°$. On the other hand, τ_{bd} changes very little with respect to θ until $\theta \approx 60°$, as seen in Figure 8. Beyond $\theta \approx 60°$, τ_{bd} increases to a maximum value, which occurs at $\theta = \theta_{cutoff}$. At $\theta > \theta_{cutoff}$, τ_{bd} decreases sharply to zero at $\theta = 90°$. Turning to the variation of ρ_{bt} with θ, it is evident from Figure 9 that ρ_{bt} remains almost constant with respect to θ until $\theta \approx 60°$. Beyond $\theta \approx 60°$, ρ_{bt} increases slightly to a maximum value at $\theta = 90°$.

Consideration will now turn to the comparison between the experimental results and the analytical model documented in EnergyPlus (DOE 2007). Figure 10 shows plots of solar properties versus θ for a 20 mesh, 0.006 in. (0.153 mm) blue-gray screen (item e in Table 1). The models generally follow the same trend as the experimental results. Furthermore, the models are in good agreement with the experimental results except for an obvious underprediction of τ_{bd} in the range of $0 < \theta < 45°$. This underprediction is small, with a maximum value of 2% in absolute terms at $\theta = 0$. Nonetheless, it can be explained by considering the accuracy of the model. As stated in EnergyPlus (DOE 2007), τ_{bb} was derived from pure geometry and as such is only influenced by the geometrical properties of the screen and θ. However, τ_{bd} was formulated by curve-fitting results from an optical ray tracing algorithm that modeled the reflectivity of the wire as diffuse. More specifically, generalised curves were fitted to accommodate ray tracing results for $0.2 \le D/S \le 0.8$ and $0.2 \le \rho^{w} \le 0.8$. Since the curve-fitted model generally underpredicts the optical ray tracing results for most screens with modest values of D/S and wire reflectivity (McCluney 2006), we expect a similar trend

Table 2. Summary of Solar Optical Properties at Normal Incidence

Item	Measurements with IS				Measurements without IS	Calculated Openness, A_o
	Beam-Total Reflectance, $\rho_{bt}(\theta=0)$	Beam-Total Transmittance, $\tau_{bt}(\theta=0)$	Beam-Diffuse Transmittance, $\tau_{bd}(\theta=0)$	Beam-Beam Transmittance, $\tau_{bb}(\theta=0)$	Beam-Beam Transmittance, $\tau_{bb}(\theta=0)$	
a	0.23	0.44	0.08	0.36	0.38	0.37
b	0.19	0.54	0.08	0.46	0.47	0.48
c	0.18	0.54	0.05	0.49	0.48	0.48
d	0.18	0.60	0.08	0.52	0.54	0.54
e	0.07	0.65	0.02	0.63	0.64	0.65
f	0.01	0.71	0.01	0.70	0.73	0.73

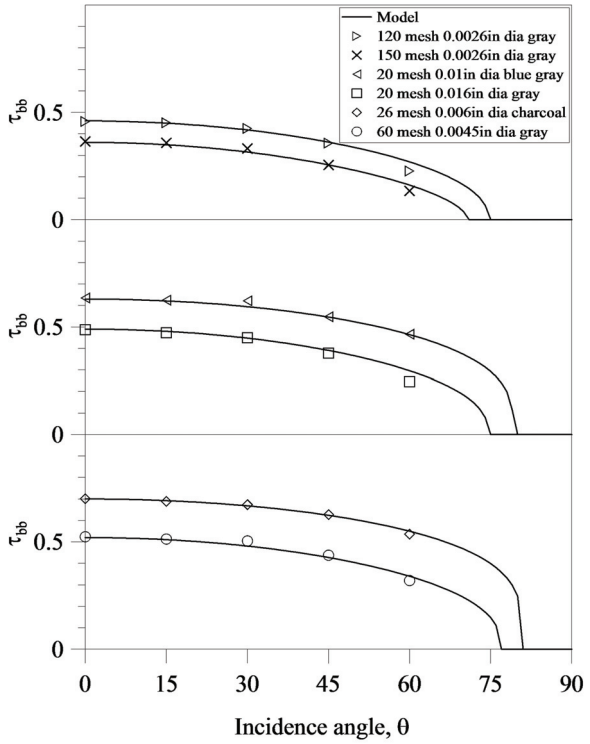

Figure 6 *Beam-beam transmittance versus incidence angle.*

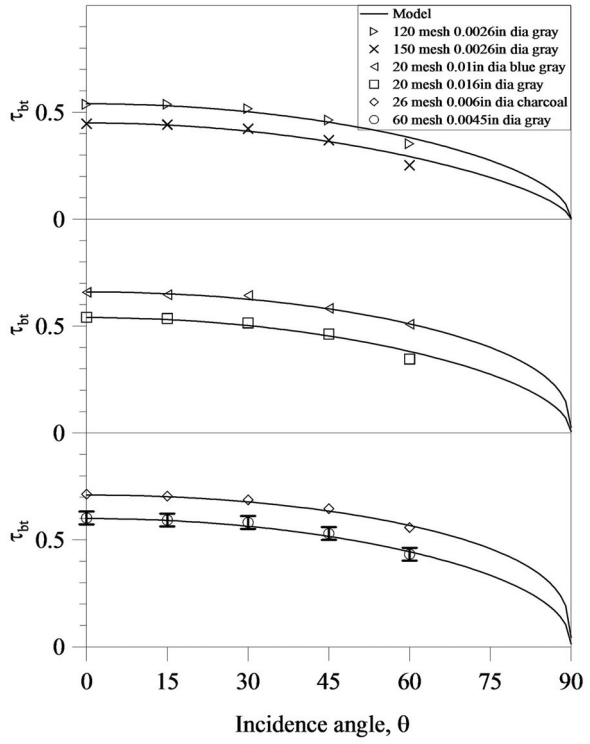

Figure 7 *Beam-total transmittance versus incidence angle.*

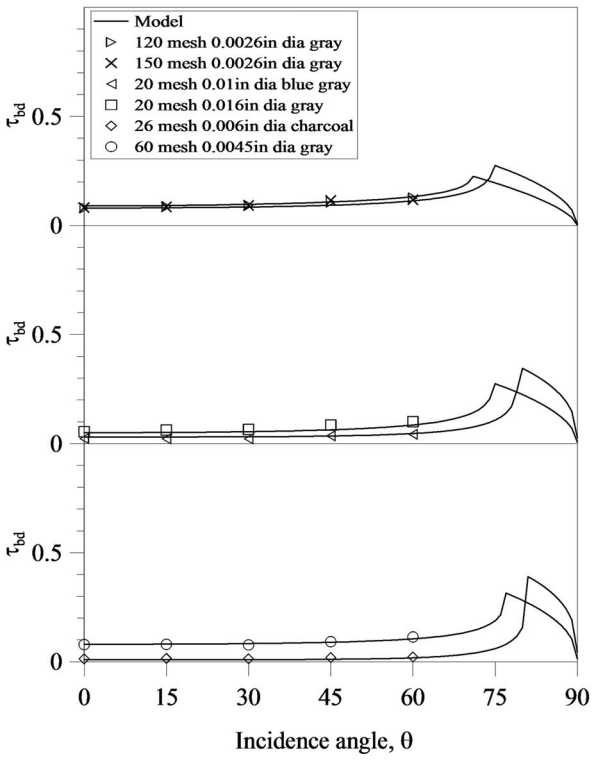

Figure 8 *Beam-diffuse transmittance versus incidence angle.*

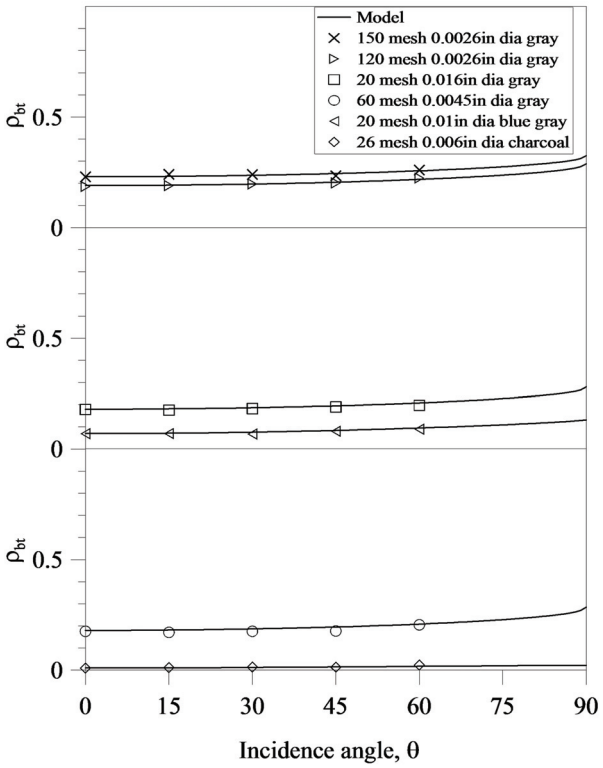

Figure 9 *Beam-total reflectance versus incidence angle.*

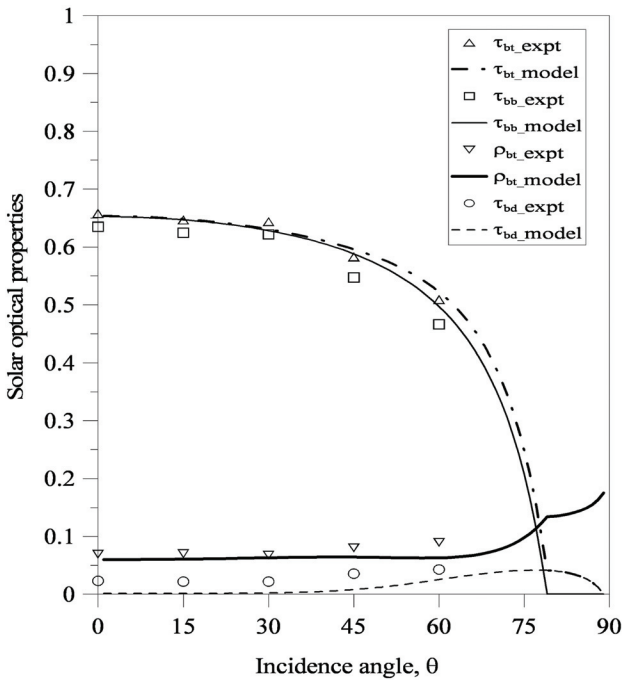

Figure 10 *Comparison between experimentally determined solar optical properties and EnergyPlus models for 20 mesh blue-gray screen.*

between the curve-fitted model and results obtained from the measurements. It should be noted that the agreement between EnergyPlus models and the measurement results for all other screens considered in this study was also good.

CONCLUSIONS

Off-normal solar optical properties of shading devices are particularly useful in estimating the influence of these devices on solar gain. Experimental determination of the off-normal solar optical properties of insect screens is reported in this study. Such screens frequently attached to windows are classified as shading devices since they have significant influence on solar gain. The experiments involve the use of special sample holders attached to an integrating sphere of a spectrophotometer. Semi-empirical models were subsequently developed from the experimental results. Given solar optical properties obtained at normal incidence, the proposed semi-empirical models can be used to obtain the off-normal properties of any screen. To further demonstrate the reliability of the measurement technique, the experimental results were compared to analytical and ray tracing models recently developed for building energy simulation. In general, there was very good agreement between the two sets of results.

ACKNOWLEDGMENTS

Natural Sciences and Engineering Research Council of Canada and American Society of Heating, Refrigerating and Air-Conditioning Engineers, Inc., are gratefully acknowledged for their financial support.

NOMENCLATURE

Symbols

A_o = openness
D = wire diameter, in. (mm)
S = wire spacing, in. (mm)
b = exponent in semi-empirical models

Greek Letters

ρ = reflectance (dimensionless)
τ = transmittance (dimensionless)
θ = incidence angle

Subscripts

bb = beam-beam optical property
bd = beam-diffuse optical property
bt = beam-total optical property
dd = diffuse-diffuse optical property

Superscripts

norm = normalised solar optical property
w = wire solar optical property

REFERENCES

ASTM. 1987. *ASTM E891-87, Standard Tables for Terrestrial Direct Normal Solar Spectral Irradiance for Air Mass 1.5*. Philadelphia: American Society for Testing and Materials.

ASTM. 1996. *ASTM E903-96, Standard Test Method for Solar Absorptance, Reflectance, and Transmittance of Materials Using Integrating Spheres*. Philadelphia: American Society for Testing and Materials.

Brunger, A., F.M. Dubrous, and S.J. Harrison. 1999. Measurement of the solar heat gain coefficient and U-value of windows with insect screens. *ASHRAE Transactions* 105(2):1038–44.

DOE. 2004. *2004 Buildings Energy Data Book*. Washington, DC: U.S. Department of Energy.

DOE. 2007. *EnergyPlus Engineering Reference—The Reference to EnergyPlus Calculations*. Washington, DC: U.S. Department of Energy.

Farber, E.A., W.A. Smith, C.W. Pennington, and J.C. Reed. 1963. Theoretical analysis of solar heat gain through insulating glass with inside shading. *ASHRAE Journal,* pp. 79.

Grasso, M., and D.R. Buchanan. 1982. Window shades in energy conservation. *Home Economics Research Journal* 11:89–97.

Harrison, S.J., and S.J. van Wonderen. 1998. Evaluation of solar heat gain coefficient for solar-control glazings and shading devices. *ASHRAE Transactions* 104(1b): 1051–62.

Kotey, N.A., M.R. Collins, J.L. Wright, and T. Jiang. 2008. A simplified method for calculating the effective solar optical properties of a venetian blind layer for building energy simulation. *ASME Journal of Solar Energy Engineering*. Forthcoming in the May issue.

Kotey, N.A., J.L. Wright, and M.R. Collins. 2009a. Determining off-normal solar optical properties of drapery fabrics. *ASHRAE Transactions* 115(2).

Kotey, N.A., J.L. Wright, and M.R. Collins.2009b. Determining off-normal solar optical properties of roller blinds. *ASHRAE Transactions* 115(1).

McCluney, R., with Florida Solar Energy Centre, FL. Personal email with the author, 2006.

Parmelee, G.V., and W.W. Aubele. 1952. The shading of sunlit glass: An analysis of the effect of uniformly spaced flat opaque slats. *ASHVE Transactions* 58:377–98.

Pfrommer, P., K.J. Lomas, and Chr. Kupke. 1996. Solar radiation transport through slat-type blinds: A new model and its application for thermal simulation of buildings. *Solar Energy* 57(2):77–91.

Wright, J.L., and N.A. Kotey. 2006. Solar absorption by each element in a glazing/shading layer array. *ASHRAE Transactions* 112(2):3–12.

Yahoda, D.S., and J.L. Wright. 2005. Methods for calculating the effective solar-optical properties of a venetian blind layer. *ASHRAE Transactions* 111(1):572–86.

APPENDIX

Table A.1. Beam-Beam Transmittance from Measurements

Incidence Angle, °	Beam-Beam Transmittance					
	Item a	Item b	Item c	Item d	Item e	Item f
0	0.36	0.46	0.49	0.52	0.63	0.70
15	0.36	0.45	0.47	0.51	0.62	0.69
30	0.33	0.43	0.45	0.50	0.62	0.67
45	0.25	0.36	0.38	0.44	0.55	0.63
60	0.13	0.23	0.25	0.32	0.47	0.54

Table A.2. Beam-Total Transmittance from Measurements

Incidence Angle, °	Beam-Total Transmittance					
	Item a	Item b	Item c	Item d	Item e	Item f
0	0.45	0.54	0.54	0.60	0.66	0.71
15	0.44	0.54	0.54	0.59	0.65	0.70
30	0.42	0.52	0.52	0.58	0.64	0.69
45	0.37	0.46	0.46	0.53	0.58	0.65
60	0.25	0.35	0.35	0.43	0.51	0.56

Table A.3. Beam-Diffuse Transmittance from Measurements

Incidence Angle, °	Beam-Diffuse Transmittance					
	Item a	Item b	Item c	Item d	Item e	Item f
0	0.08	0.08	0.05	0.08	0.02	0.01
15	0.08	0.09	0.06	0.08	0.02	0.02
30	0.09	0.09	0.07	0.08	0.02	0.01
45	0.11	0.11	0.08	0.09	0.04	0.02
60	0.12	0.13	0.10	0.11	0.04	0.02

Table A.4. Beam-Total Reflectance from Measurements

Incidence Angle, °	Beam-Total Reflectance					
	Item a	Item b	Item c	Item d	Item e	Item f
0	0.23	0.19	0.18	0.18	0.07	0.01
15	0.24	0.19	0.18	0.17	0.07	0.01
30	0.24	0.20	0.18	0.18	0.07	0.01
45	0.23	0.20	0.19	0.18	0.08	0.01
60	0.26	0.22	0.20	0.21	0.09	0.02